Implementation of a Nonlinear Planar Magnetics Model

Lew Andrew Ravelas Tria, *Member, IEEE*, Daming Zhang, *Member, IEEE*, and John E. Fletcher, *Senior Member, IEEE*

***Abstract*—A nonlinear lumped element model for planar magnetics is presented. This technique develops an equivalent circuit model for multilayer planar magnetic components using 1-D analysis of Maxwell's equations. Conducting layers are represented as impedance networks, while the insulating regions are modeled as air-cored inductors. The equivalent circuit model is extended by representing the nonlinear magnetic core material as a nonlinear impedance whose magnetization characteristic is based on the Jiles–Atherton hysteresis model as well as modeling skin and proximity effects in the conductors and current distribution across windings, the improved model also integrates hysteresis loss of the magnetic core and saturation effects. The technique can be implemented in circuit simulation software. A prototype planar transformer, using printed circuit boards to mount windings, was characterized to validate the performance of the model. It is demonstrated that the developed nonlinear model more accurately represents the characteristics of the experimental transformer compared to the existing linear lumped element model. This includes the effect of core saturation on the input current and output-voltage waveforms. The technique is generalized and can be applied to many topologies and geometries.**

***Index Terms*—Jiles–Atherton model, nonlinear magnetics equivalent circuit, planar magnetics, printed circuit board (PCB) transformer.**

I. Introduction

PLANAR magnetics are widely used in high-frequency power electronic converters in order to achieve high-power density supplies. With larger surface areas, planar transformers offer better thermal performance compared to conventional magnetics. Using windings that are preformed on, for example, printed circuit boards (PCBs), planar magnetics can be mass-manufactured and integrated with circuitry with high repeatability. In addition, thinner and wider conductors assist in reducing high-frequency losses due to skin and proximity effects. Due to these advantages, numerous studies have modeled planar transformers and inductors to predict and characterize their performance and to improve their design.

Many of the studies have concentrated on modeling winding loss in high-frequency applications. The majority of these models are based on the numerical model developed by Dowell [1] for conventional transformers and applied to planar magnetics [2], [3] and nonsinusoidal current wave shapes [4]–[6]. These models are able to capture some of the parasitic components of the windings, particularly the winding resistance and leakage inductance. Other studies derived equivalent circuits of the planar magnetic structure-based directly on 1-D analysis of Maxwell's equations. These studies include models based on transmission lines [9] and optical systems analogies [10]. A more intuitive and systematic approach to model planar magnetics was presented in [8]. Although differing in the approach taken, all of these planar magnetics models enable the representation of multilayer magnetic structures with lumped element models, which can be implemented in circuit simulation software. With this type of model, proximity and skin effects, and current distribution among windings can be predicted with less intensive computation than that required by finite element analysis (FEA) software. For example, in [11], the current sharing in a multilayer transformer was simulated using a lumped element model in circuit simulation software and demonstrated a 60-fold reduction in computation time compared to FEA software, while producing similar results. However, most of these lumped element models concentrate on determining the winding loss of the magnetic component. This is understandable, since in high-power and high-frequency applications, winding losses are usually more significant. In these lumped element models, the core is represented as a lossless and linear component. In linear models, the hysteresis and magnetic core losses are not considered. In some cases, a loss component is added with a core impedance that represents any loss unaccounted for the total component loss [12], but nonlinear characteristics are still not considered.

To model the dynamic and transient response of a magnetic component, such as inrush current, subharmonic, and chaotic responses, the hysteresis of the magnetic core should be included in a model. A number of studies show the advantage of using a hysteresis model for dynamic system response [13]–[16]. However, most of these studies are used for low-frequency applications. For high-frequency models, winding loss was considered as single loss impedance, if not neglected. The most commonly used method to model hysteresis is the Jiles–Atherton (J–A) model [17], which is adopted for this study. The J–A model was chosen because of its systematic representation of the hysteresis characteristic using first-order differential equations, which can

Manuscript received June 3, 2015; revised October 13, 2015 and August 10, 2015; accepted November 17, 2015. Date of publication November 25, 2015; date of current version March 25, 2016. The work of L. A. R. Tria was supported by the Engineering Research and Development for Technology—Faculty Development Program of the University of the Philippines and the Department of Science and Technology, Philippines. Recommended for publication by Associate Editor J. Acero.

L. A. R. Tria is with the School of Electrical Engineering and Telecommunications, University of New South Wales, Sydney, N.S.W. 2052, Australia and also with the Electrical and Electronics Engineering Institute, University of the Philippines Diliman, Quezon City 1101, Philippines (e-mail: lew.tria@student.unsw.edu.au).

D. Zhang and J. E. Fletcher are with the School of Electrical Engineering and Telecommunications, University of New South Wales, Sydney, N.S.W. 2052, Australia (e-mail: daming.zhang@unsw.edu.au; john.fletcher@unsw.edu.au).

Color versions of one or more of the figures in this paper are available online at http://ieeexplore.ieee.org.

Digital Object Identifier 10.1109/TPEL.2015.2503744

be solved easily with minimum computational requirements. Previous works have incorporated the J–A model to simulate hysteresis of magnetic components, such as EMI filters [19], [20] and transformers [21] in various software platforms. However, these works involve models for conventional wire-wound devices and model the magnetics as a single core.

This paper presents a nonlinear planar magnetics model that incorporates hysteresis characteristics into the lumped element models presented in [8] and [10], which use a linear magnetic core model. Although it was suggested in [8], to the best knowledge of the authors, there has been no previous effort to incorporate a hysteresis model to the linear lumped element models for multilayer planar magnetics. An added novelty of this method is that the top and bottom limb of the transformer core are modeled separately, which enables modeling of customized core geometry and materials, for example, two half-cores with different material properties. The incorporation of the nonlinear core model into the lumped element model integrates both the magnetic core's hysteresis loss and saturation effects, together with the numerous advantages and capabilities of the existing linear model, such as computation of winding loss and current distribution in the windings. This systematic model can be implemented in circuit simulation software like Simulink, which provides a faster and cheaper alternative to FEA simulation software. The performance of the model is validated by experimental results using a prototype planar transformer. The model was able to replicate the nonlinear behavior and saturation effects of the experimental transformer including nonsinusoidal magnetizing current.

The paper is presented as follows. Section II presents the linear lumped element model used as basis of this paper. Section III reviews the J–A model and incorporates it within the lumped element model. The model's implementation is described in Section IV. Simulation results and comparison with the experimental results are presented in Section V. Section VI concludes the paper.

II. Linear Lumped Element Model for Planar Magnetics

A linear lumped model developed in [8] and [10] for planar magnetics is reviewed in this section. A multilayer planar magnetic component can be represented by an equivalent circuit model whose impedances are calculated directly from 1-D-analysis of Maxwell's equations. The model is based on the assumption that the electromagnetic fields are parallel (tangential) inside and between layers, as shown in Fig. 1(a). The lumped element model is developed from a model of this single layer and then repeated to model multilayer systems.

A. Single-Turn Conductor

Fig. 1(a) shows a single-turn conductor of length *d* and width *w*. A voltage *V* is applied across the terminals of the conductor layer and current *I* flows through the conductor. E_T and E_B are the electric field running along the length on the top and bottom faces of the conductor, respectively, while H_T and H_B are the magnetic field along the width of the conductor, on the top and bottom faces of the conductor, respectively. Solving the Helmholtz equation and using Ampere's law yields a set of equations, which captures the relationship between the *E* and *H* field in (1) and (2) [23], which can be represented by the three-port impedance network, Fig. 1(b). The values of the impedances in Fig. 1(b) depend on the layer geometry and material properties given in (3)

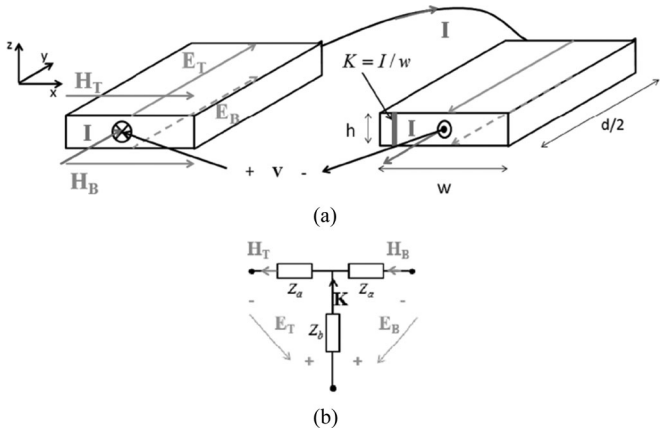

Fig. 1. (a) One-turn conducting layer showing dimensional details and *E* and *H* fields and (b) equivalent three-port impedance network of the single turn [8].

$$E_T = Z_a H_T + Z_b (H_T - H_B) \tag{1}$$

$$E_B = Z_b (H_T - H_B) - Z_a H_B \tag{2}$$

$$Z_{ai} = \frac{\gamma(1 - e^{-\gamma h_i})}{\sigma(1 + e^{-\gamma h_i})}; \quad Z_{bi} = \frac{2\gamma e^{-\gamma h_i}}{\sigma(1 - e^{-2\gamma h_i})} \tag{3}$$

where $\gamma = (1 + j)/\delta$ is the propagation constant, $\delta = \sqrt{2/(\mu_r \mu_0 \omega \sigma)}$ is the skin depth of the material at the angular frequency, ω, μ_0 is the permeability of free space, μ_r is the material's relative permeability, σ is the material's conductivity, and h_i is the layer thickness.

B. Layer Ports

A layer port is the interface between the electrical and electromagnetic domain. The layer ports also allow connection between layers. In [10]–[12], a coupler is used with ratio of $m_i\sqrt{d/w}$, where m_i is the number of series-connected turns in layer *i*. On the other hand, it is represented in [7] and [8] by an ideal transformer with turns ratio, $m_i : 1$. Both representations serve the same purpose of coupling the electrical input to the electromagnetic fields, except that for the latter, all signals are in the circuit domain, represented by currents and voltages.

C. Nonconducting Layers

Spacings and insulators are modeled by the impedance in (4), where a_i is the thickness of the space or insulator between layer *i* and layer *i + 1*

$$Z_{Si} = j\omega\mu_0 a_i. \tag{4}$$

The magnetic core layer is represented by a single impedance

$$Z_{Fi} = j\omega\mu_0\mu_r h_{Fi} \tag{5}$$

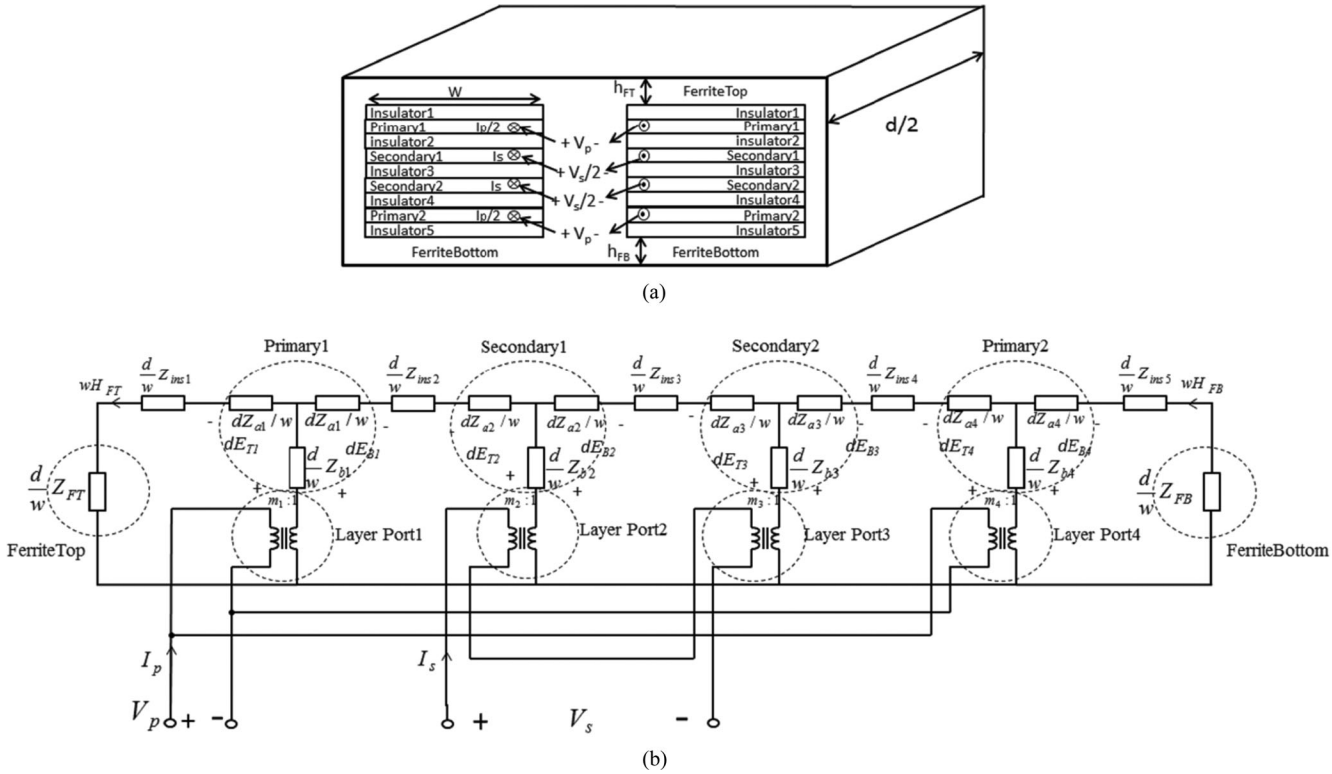

Fig. 2. Lumped circuit representation of a multilayer planar transformer. The primary windings are connected in parallel, while the secondary windings are connected in series. (a) Physical transformer and (b) the lumped element representation as presented in [8].

where h_{Fi} is the thickness of either the top or bottom of the core and μ_r is the relative permeability of the core material.

D. Modeling Multilayer Structures

The impedance networks are connected side-by-side as they are arranged in the layer stack. Conducting layers connected by cross-layer structures are represented by connecting their input ports according to how they are connected in the physical system. Thus, a magnetic structure, shown in Fig. 2(a), with two primary conducting layers in parallel and two secondary conducting layers in series, can be modeled as in Fig. 2(b). Here the impedances are multiplied by a factor of *d/w*, magnetic fields by *w*, and electric fields by *d*, to convert the electromagnetic system to electric circuit domain for implementation in circuit simulation software.

E. Assumptions and Limitations of the Existing Lumped Element Model

The linear lumped element model presented in [8] and [10] assumed that the legs of the core are short relative to the winding breadth, and the core made of high-permeability material. Thus, in computing Ampere's law, it only considers the magnetic field in the top and bottom part of the layers including the magnetic core. However, for commercially available planar E-cores, the core height is still significant and neglecting; it gives a large deviation from actual measurements, as will be presented in Section V.

In addition, the model only considered linear core characteristics and loss-less impedances. As will be presented in Section V, at high excitation, the existing linear lumped element model cannot accurately represent the response of an experimental transformer. A major contribution of this paper is the incorporation of the nonlinear characteristic of a magnetic material in the linear lumped element model. With the proposed model, hysteresis and saturation characteristics of magnetic materials can be demonstrated and core loss can be derived. For this, the J–A hysteresis model will be utilized as will be explained.

III. J–A Hysteresis Model

The nonlinear characteristic of the magnetic core is modeled using the J–A hysteresis model [17], [18]. A review of the hysteresis model is presented in this section. The J–A model uses the magnetic field *H* as the independent variable and magnetization *M* as the dependent variable. In the model, the total magnetization *M* is composed of an irreversible and reversible component

$$M = M_{irr} + M_{ev} \tag{6}$$

where M_{irr} is the irreversible magnetization and M_{ev} is the reversible magnetization.

The derivative of the irreversible magnetization against magnetic field intensity is given by

$$\frac{dM_{irr}}{dH} = \frac{M_{an} - M_{irr}}{k \cdot sign\left(\frac{dH}{dt}\right) - \alpha\left(M_{an} - M_{irr}\right)} \tag{7}$$

where *sign* is defined as *sign* $(x) = 1$ for $x \geq 0$ and $sign(x) = -1$ for$x < 0$. H_e is the effective magnetic field which is expressed as

$$H_e = H + \alpha M \tag{8}$$

where α is the interdomain coupling factor.

M_{an} is the anhysteretic magnetization and described using the Langevin function

$$M_{an} = M_s \left(\coth \frac{H_e}{a} - \frac{a}{H_e} \right) \tag{9}$$

$$\frac{\partial M_{an}}{\partial H_e} = \frac{M_s}{a} \left[1 - \coth^2 \left(\frac{H_e}{a} \right) + \left(\frac{a}{H_e} \right)^2 \right] \tag{10}$$

where M_s is the saturation magnetic moment of the core material and *a* is a shape parameter called domain density.

The derivative of the reversible magnetization against magnetic field is

$$\frac{dM_{rev}}{dH} = c \left(\frac{dM_{an}}{dH} - \frac{dM}{dH} \right) \tag{11}$$

where *c* is the reversibility factor.

Using (6)–(11), the derivative of magnetization against magnetic field can be derived as follows:

$$M_{rev} = c\,(M_{an} - M) \tag{12}$$

$$\frac{dM}{dH} = \frac{1}{1+c} \frac{M_{an} - M_{irr}}{sign\left(\dot{H}\right) \cdot k - \alpha\,(M_{an} - M_{irr})} + \frac{c}{1+c} \frac{dM_{an}}{dH} \tag{13}$$

where $M_{an} - M_{irr}$ can then be expressed as $(1+c)$ $(M_{an} - M)$ and *k* corresponds to pinning factor.

When using the equation $M_{rev} = c\,(M_{an} - M_{irr})$ instead of (12), (13) can be expressed as (14) instead

$$\frac{dM}{dH} = (1-c)\,\delta \frac{M_{an} - M}{sign\left(\dot{H}\right) k\,(1-c) - \alpha\,(M_{an} - M)} + c \frac{dM_{an}}{dH} \tag{14}$$

where

$$\delta = \begin{cases} 0, & \text{if } sign\left(\dot{H}\right) \cdot (M_{an} - M) \leq 0; \\ 1, & \text{otherwise.} \end{cases} \tag{15}$$

The flux density *B* can be computed as

$$B = \mu_0\,(H + M) \tag{16}$$

where μ_0 is the permeability of free space. The time-derivative of the flux is

$$\frac{d\Phi}{dt} = \mu_0 A_c \frac{d\,(H+M)}{dt} = \mu_0 A_C \frac{dH}{dt} \left(1 + \frac{dM}{dH} \right) \tag{17}$$

where A_c is the cross-sectional area of the core perpendicular to the magnetic path and

$$\frac{dM}{dt} = \frac{dM}{dH} \cdot \frac{dH}{dt} \tag{18}$$

can be solved using (14). In the above equations, *a*, α, *c*, *k,* and M_s are J–A parameters, which will be determined by curve fitting of measured hysteresis curves, as will be described in the following section.

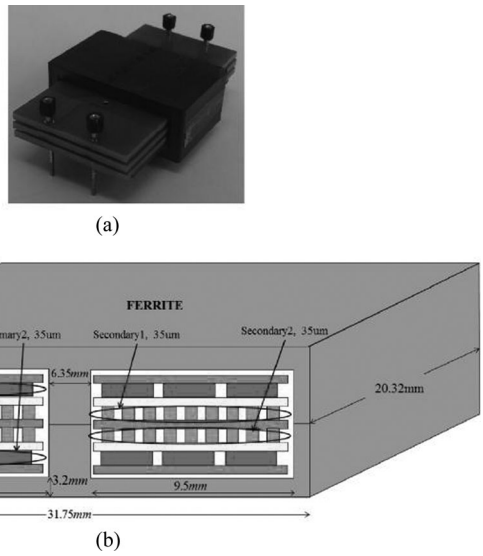

Fig. 3. Prototype planar transformer. (a) Actual transformer prototype and (b) transformer geometry and winding arrangement. The magnetic path length, $l_m = 41.7$ mm and the cross-sectional area of the center leg $A_C = 126$ mm^2.

In the derivation of the impedance of the magnetic core in (5), only the magnetic field through the core H_F was considered and the EMF was computed as in

$$\frac{d\Phi}{dt} = \frac{dBA}{dt} = d\mu_0 \mu_r h_F \frac{dH_F}{dt}. \tag{19}$$

To account for the hysteretic characteristics of magnetic materials, we propose to include the magnetization *M* using (16) instead and the resulting EMF will be

$$\frac{d\Phi}{dt} = \frac{dBA}{dt} = d\mu_0 h_F \frac{d\,(H_F + M)}{dt}. \tag{20}$$

IV. Model Implementation and Verification

A. Experimental Setup

A high-frequency low-profile transformer with a turns ratio of 1:6, was used to obtain experimental data. Fig. 3(a) shows the prototype transformer used to obtain experimental data. The winding was made of three double-sided 1.6 mm FR4 PCB with 35-μm-thick copper traces. PCBs were separated by 0.5-mm-thick insulators. The primary winding is composed of two sets of parallel connected windings, each with three turns of 2.4–mm-wide copper traces. The secondary winding is composed of 18 turns of 0.4-mm-wide copper traces in two layers. The windings are interleaved in a P-S-S-P configuration. The magnetic core is a planar E–E core with dimensions shown in Fig. 3(b).

To acquire the *B–H* curve of the magnetic core, the experimental setup in Fig. 4 was utilized. A sinusoidal input voltage is supplied by a signal generator driving a power amplifier. The secondary voltage v_s and primary current i_p are obtained using an oscilloscope with voltage and current probes and data processed in MATLAB.

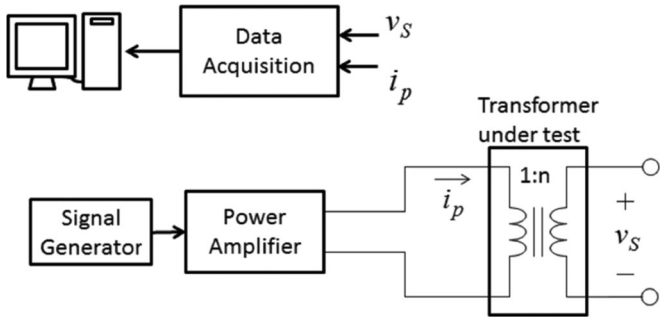

Fig. 4. Experimental setup for acquiring magnetic field and flux density.

The magnetic field was derived directly from the input current i_p as the secondary side is left open-circuited, using

$$H_j = \frac{N_p i_{p,j}}{l_m} \tag{21}$$

where N_p is the number of turns in the primary and l_m is the magnetic path length of the core (41.7 mm). The flux density is derived from the Faraday's law, using the secondary voltage v_s referred to the primary side, to discount the effect of the winding series impedance

$$B_j = \frac{1}{NA_c} \sum \frac{V_{s,j}}{n} \Delta t \tag{22}$$

where A_c is the cross-sectional area of the center leg of the core, *N* is the number of turns in the primary, *n* is the turns ratio, and Δt is the sampling time.

B. Implementation of the Nonlinear Model

The transformer in Fig. 3 was modeled in Simulink, as shown in Fig. 6. For the primary and secondary windings layers, (3) was used, while for the insulators and PCB layers, (4) was used. Instead of (5), nonlinear impedances, *CoreTop* and *CoreBottom* were used to represent the top and bottom part of the magnetic core, respectively. The J–A model implementation, outlined in Fig. 5, was adopted and modified from [14]. For consistency with the definition of the J–A model presented in Section III, *H* was used as the independent variable instead, while *M* and *B* are the dependent variables. This was implemented as a nonlinear impedance using controlled voltage source shown in Fig. 6(b). The control current represents the magnetic field through the core, wH_{FT} or wH_{FB}. The voltage output is the electromotive force (EMF) computed using (20). The J–A parameters used to implement the model are shown in Table I. The parameters were derived by curve-fitting experimental *B–H* curves using a differential evolution-based algorithm as described in previous work [16], [22]. The input to the model is a sinusoidal voltage source $V_{\rm pri}$ which simulates the experimental primary voltage with variable amplitude and variable frequency.

V. Model Validation

An open-circuit test was conducted to acquire $V_{\rm sec}$ and $I_{\rm pri}$ in Fig. 6, by applying a sinusoidal voltage $V_{\rm pri}$ with similar amplitude and frequency to the experimental input voltage. Fig. 7 shows the simulation results of the model using Fig. 6(b), a modified model that will be explained subsequently, and their comparison with experimental measurements. The output voltage of both models shows good agreement with experimental results. However, a large deviation was found between the original model and experimental primary current, as can be seen in the lower half of the Fig. 7. This result was expected since in the formulation of the original lumped element model, only the

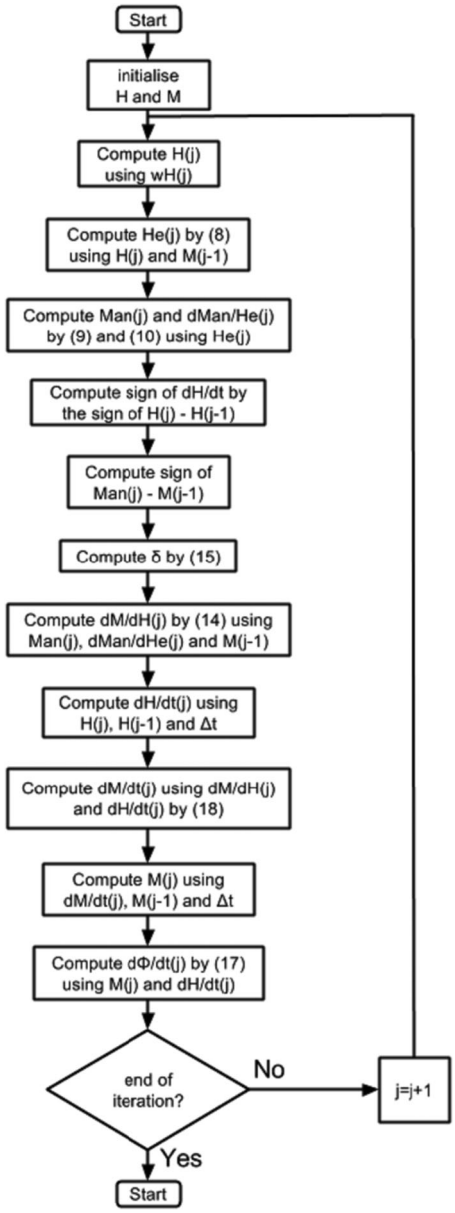

Fig. 5. Flowchart for implementing the J–A model.

TABLE I
J–A Parameters

a, *A/m*	α, *1E-6*	c	k, *A/m*	Ms, *kA/m*
38	18	0.61	35	433

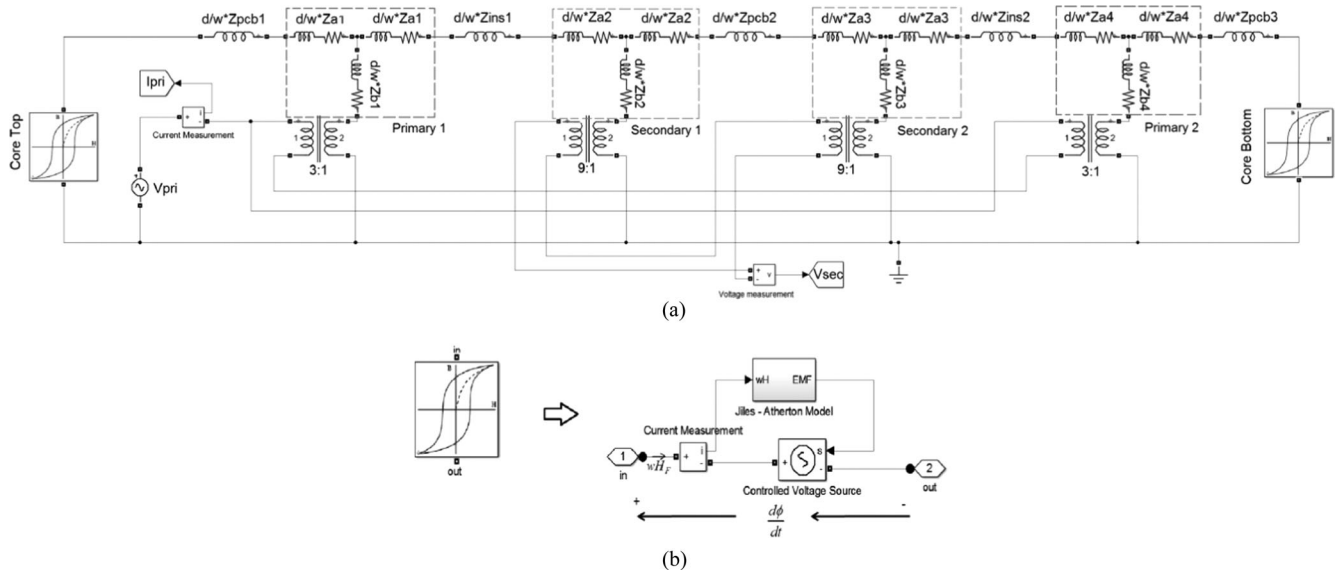

Fig. 6. (a) Implementation of the planar transformer model in Simulink. $V_{\rm pri}$ is a sinusoidal voltage source with variable voltage and frequency. Equivalent model of the prototype PCB transformer. (b) Implementation of the nonlinear impedance for the core layer.

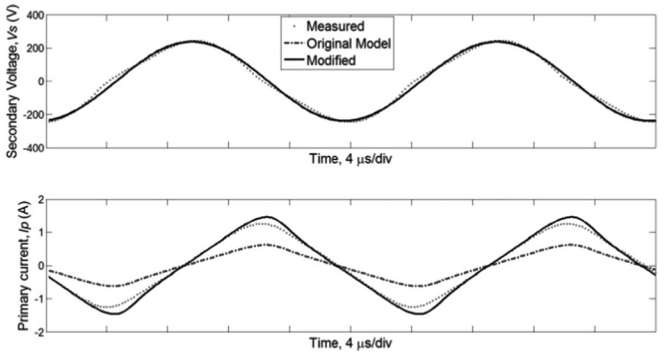

Fig. 7. Comparison of measured secondary voltage and primary current with original and modified nonlinear model's response. Input voltage $V_p = 40$ V, frequency $f = 50$ kHz.

magnetic fields in the top and bottom limb of the transformer are considered in [8]. It was assumed that the vertical legs are composed of high-permeability materials and their lengths are small. For instance, the magnetic component in Fig. 8(a) is modeled in Fig. 8(b) using this assumption. Summing the currents in Fig. 8(b) shows that $mI_1 = w(H_{FT} - H_{FB})$. The effective magnetic path length is only twice the winding breadth width w. This will be a valid assumption as long as the lengths of the vertical limbs are significantly smaller than the width of the core, which is not the case in the experimental transformer core.

To consider the vertical limbs, the current through the nonlinear impedance in Fig. 8(b) can be assumed to be $(w + s)H_F$ instead. In this modified model, summing the currents shows $mI_1 = (w + s)(H_{FT} - H_{FB})$, with the magnetic path length $l_m = 2(s + w)$. Thus, for the implementation of the J–A model in Fig. 5, the magnetic field H is computed by dividing the current by $(w + s)$ instead of just w. After modification, the response of the model improved as shown in Fig. 7.

Fig. 9 shows the comparison between the modified nonlinear planar magnetics model, experimental measurements, and the

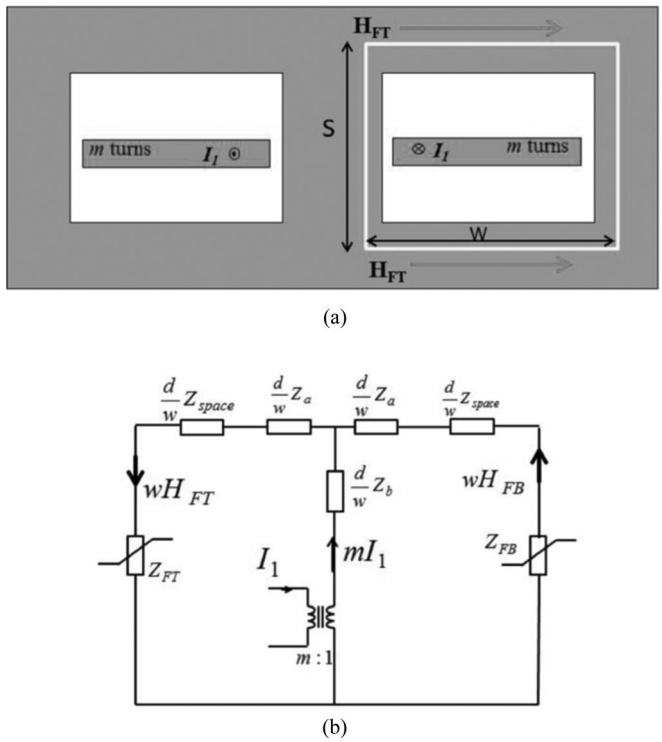

Fig. 8. Planar magnetics with single layer of m-turn winding. (a) Physical transformer showing magnetic path length l_m and directions of magnetic field. (b) original model representation. Z_a, $Z_b Z_{\rm b}$, and $Z_{\rm space}$ are impedances given by (3) and (4).

original linear lumped element model output at different input voltages. It can be seen that the linear and nonlinear model gave similar response with the experimental results at lower excitation levels. However, as the excitation is increased, nonlinearity in the experimental measurements becomes apparent and the linear model's output deviates from the experiment, particularly the primary current. The developed nonlinear model's response

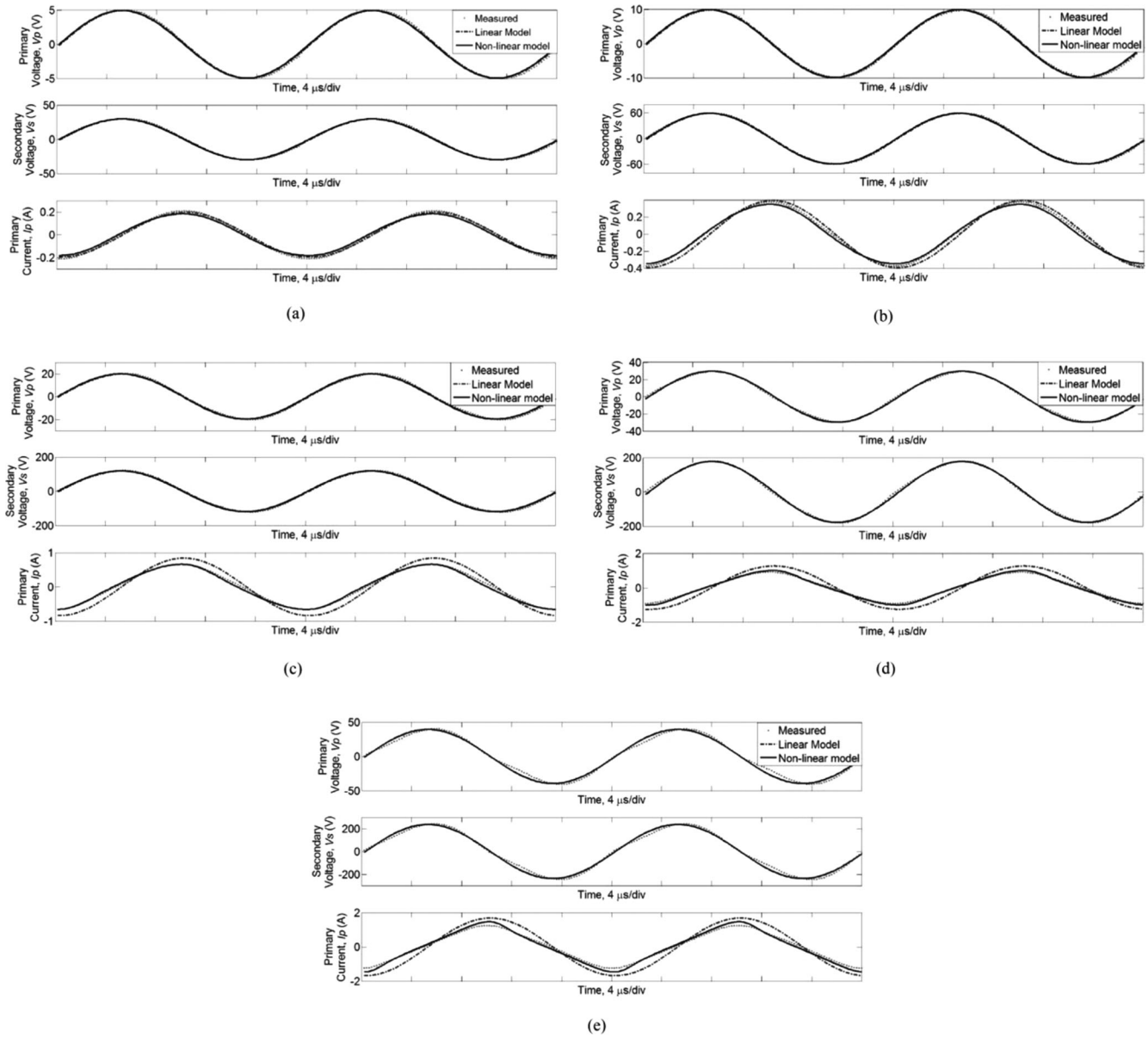

Fig. 9. Comparison between experimental measurement, linear model's and developed nonlinear model's responses at various input voltage, frequency, $f =$ 50 kHz. (a) $V_p = 5\ \mathrm{V_{pk}}$, (b) $V_p = 10\ \mathrm{V_{pk}}$, (c) $V_p = 20\ \mathrm{V_{pk}}$, (d) $V_p = 30\ \mathrm{V_{pk}}$, and (e) $V_p = 40\ \mathrm{V_{pk}}$.

replicates the nonlinear characteristic of the experimental measurements, as evident in Fig. 9. It was observed that the experimental primary voltage exhibited nonlinear characteristics at high-excitation levels, attributed to the limit in the power amplifier used. To accurately simulate these cases, the experimental input current was used in the simulation as excitation signal by replacing V_{pri} in Fig. 6(a) with a current source. Fig. 10 shows the response of the developed model compared to the experimental results and the response of the linear lumped element model using an experimental primary current as the excitation signal. The developed nonlinear model replicates the experimental measurements even with nonsinusoidal input current, which the linear lumped model fails to do. It should be noted, however, that the implementation of the nonlinear impedance

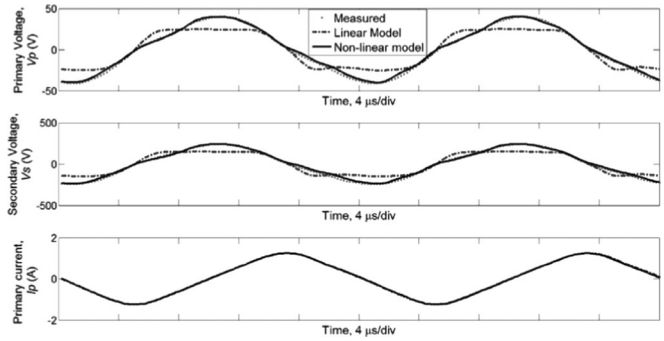

Fig. 10. Comparison between experimental measurement, linear model's and nonlinear model's responses using experimental primary current as excitation signal to the model, $f =$ 50 kHz.

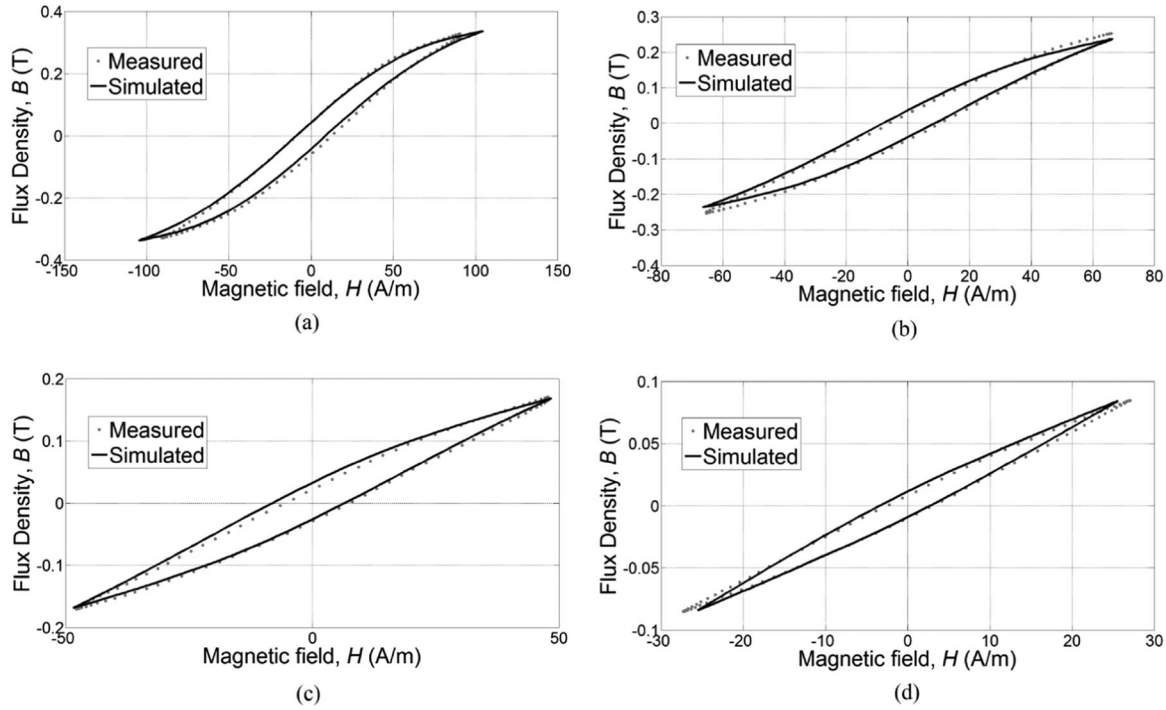

Fig. 11. Comparison of flux density versus magnetic field curves for various input voltage, V_p frequency, $f = 50$ kHz. (a) $V_p = 40\ \mathrm{V_{pk}}$, (b) $V_p = 30\ \mathrm{V_{pk}}$, (c) $V_p = 20\ \mathrm{V_{pk}}$, and (d) $V_p = 10\ \mathrm{V_{pk}}$.

added complexity to the model and hence results in longer simulation times compared to the linear lumped element model. For instance, a 1 ms simulation time at 5 $\mathrm{V_{pk}}$ excitation of the nonlinear model requires ten times more computation time than the linear model. The nonlinearity of the developed model was also validated by obtaining the *B–H* curve of the model's open circuit output using (21) and (22). The model's *B–H* curve shows good agreement with experimental results as shown in Fig. 11. Deviations with the experimental measurements can be attributed to the accuracy of acquiring the J–A parameters used to build the model.

VI. Conclusion

This paper presents a technique to model nonlinear planar magnetics. It is based on a lumped element model for planar magnetics presented in [8] and [10]. The linear impedance of the magnetic core is replaced with a nonlinear impedance using the J–A hysteresis model. The model was able to replicate the nonlinear behavior and the saturation effects of the experimental transformer including nonsinusoidal magnetizing current. However, the electrical characteristics deviate from experimental measurement. This was attributed to the height of the core not being negligible compared to the width, which was a major assumption in the previous linear lumped element models. Therefore, the model was modified to account for this additional magnetic path length. Upon modification, the developed model's response was similar to experimental measurements.

In conjunction with the capabilities of the linear lumped element model, the developed model also simulates magnetic saturation effects, which can be useful for the transient studies of magnetic components. In addition, since the model captures the hysteresis curve of the core, the hysteresis component of the core loss can be readily acquired. However, these additional capabilities result in complex implementation and more computational time. The accuracy of the model is tied to the J–A parameters. Thus, accurate determination of these parameters is essential. Only the static J–A model was utilized in this study, and for better accuracy and operation over a wider range of frequencies, the dynamic J–A should be implemented. An additional capability to be investigated further is the temperature dependence.

References

[1] P. Dowell, "Effects of eddy currents in transformer windings," *Proc. Inst. Electr. Eng.*, vol. 113, no. 8, pp. 1387–1394, Aug. 1966.

[2] R. Pittini, Z. Zhang, Z. Ouyang, M. A. E. Anderson, and O. C. Thomsen, "Analysis of planar E+I and ER+I transformers for low-voltage high-current DC/DC converters with focus on winding losses and leakage inductance," in *Proc. IEEE 7th Int. Power Electron. Motion Control Conf.*, Harbin, China, 2012, pp. 488–493.

[3] Z. Ouyang, O. C. Thomson, and M. A. E. Anderson, "Optimal design and tradeoff analysis of planar transformer in high-power DC-DC converters," *IEEE Trans. Ind. Electron.*, vol. 59, no. 7, pp. 2800–2810, Jul. 2012.

[4] B. Carsten, "High frequency conductor losses in switchmode magnetics," *Power Convers. Intell. Motion*, vol. 12, no. 11, pp. 34–36, Nov. 1986.

[5] W. Hurley, E. Gath, and J. Breslin, "Optimizing the AC resistance of multilayer transformer windings with arbitrary current waveforms," *IEEE Trans. Power Electron.*, vol. 15, no. 2, pp. 369–376, Mar. 2000.

[6] J. Ferreira, "Improved analytical modeling of conductive losses in magnetic components," *IEEE Trans. Power Electron.*, vol. 9, no. 1, pp. 127–131, Jan. 1994.

[7] M. Chen, M. Araghchini, K. K. Afridi, J. H. Lang, C. R. Sullivan, and D. J. Perreault, "A systematic approach to modeling impedances and current distribution in planar magnetics," in *Proc. IEEE 15th Workshop Control Model. Power Electron.*, Jun. 2014, pp. 1–17.

[8] M. Chen, M. Araghchini, K. K. Afridi, J. H. Lang, C. R. Sullivan, and D. J. Perreault, "A systematic approach to modeling impedances and

current distribution in planar magnetics," *IEEE Trans. Power Electron.*, vol. 31, no. 1, pp. 560–580, Jan. 2016.
[9] R. Prieto, J. A. Oliver, J. A. Cobos, and M. Christini, "Magnetic component model for planar structures based on transmission lines," *IEEE Trans. Ind. Electron.*, vol. 57, no. 5, pp. 1663–1669, May 2010.
[10] J. P. Keradec, B. Cogitore, and F. Blache, "Power transfer in a two-winding transformer: From 1-D propagation to an equivalent circuit," *IEEE Trans. Magn.*, vol. 32, no. 1, pp. 274–280, Jan. 1996.
[11] X. Magueron, A. Besri, Y. Lembeye, and J. P. Keradec, "Current sharing between parallel turns of a planar transformer: Prediction and improvement using a circuit simulation software," *IEEE Trans. Ind. Appl.*, vol. 46, no. 3, pp. 1064–1071, May/Jun. 2010.
[12] A. Schellmanns, P. Fouassier, J. P. Keradec, and J. Schanen, "Equivalent circuits for transformers based on one-dimensional propagation: Accounting for multilayer structure of windings and ferrite losses," *IEEE Trans. Magn.*, vol. 36, no. 5, pp. 3778–3784, Sep. 2000.
[13] P. R. Wilson, N. Ross, and A. D. Brown, "Modeling frequency-dependent losses in ferrite cores," *IEEE Trans. Magn.*, vol. 40, no. 3, pp. 1537–1541, May 2004.
[14] E. P. Gao, D. Zhang, and J. Fletcher, "Modeling of pulse transformer with nano-second excitation source using Jiles-Atherton method," in *Proc. IEEE ECCE Asia Downunder*, Melbourne, Vic., Australia, 2013, pp. 776–780.
[15] D. W. P. Thomas, J. Paul, O. Ozgonenel, and C. Christopoulos, "Time-domain simulation of nonlinear transformers displaying hysteresis," *IEEE Trans. Magn.*, vol. 42, no. 7, pp. 1820–1827, Jul. 2006.
[16] D. Zhang, Y. Liu, and S. Huang, "Differential evolution based parameter identification of static and dynamic J-A models and its application to inrush current study in power converters," *IEEE Trans. Magn.*, vol. 48, no. 11, pp. 3482–3485, Oct. 2012.
[17] D. C. Jiles and D. L. Atherton, "Theory of ferromagnetic hysteresis," *J. Appl. Phys.*, vol. 55, no. 6, pp. 2115–2120, Mar. 1984.
[18] D. C. Jiles and D. L. Atherton, "Theory of ferromagnetic hysteresis: Determination of model parameters from experimental hysteresis loops," *IEEE Trans. Magn.*, vol. 25, no. 5, pp. 3928–3930, Sep. 1989.
[19] C. Cuellar, A. Benabou, and N. Idir, "Characterization and modeling of hysteresis for magnetic materials used in EMI filters of power converters," *IEEE Trans. Power Electron.*, vol. 29, no. 9, pp. 4911–4920, Sep. 2014.
[20] R. Mrad, G. Pillonnet, F. Morel, C. Vollaire, and A. Nagari, "Predicting the impact of magnetic components used for EMI suppression on the baseband of a power amplifier," *IEEE Trans. Power Electron.*, vol. 30, no. 8, pp. 4199–4208, Aug. 2015.
[21] S. Liu, S. Huang, and H. Chen, "Using TACS functions within EMTP to setup current-transformer model based on the Jiles–Atherton theory of ferromagnetic hysteresis," *IEEE Trans. Power Del.*, vol. 22, no. 4, pp. 2222–2227, Oct. 2007.
[22] D. Zhang and J. E. Fletcher, "Double-frequency method using differential evolution for identifying parameters in the dynamic Jiles–Atherton model of Mn-Zn ferrites," *IEEE Trans. Instrum. Meas.*, vol. 62, no. 2, pp. 460–466, Feb. 2013.
[23] M. K. Kazimierczuk, "Winding resistance at high frequencies," in *High-Frequency Magnetic Components*, 2nd ed. West Sussex, U.K.: Wiley, 2014, pp. 265–280.

Lew Andrew Ravelas **Tria** (S'08–M'09) received the B.S. degree in electronics and communications engineering, and the M. S. degree in electrical engineering from the University of the Philippines Diliman, Quezon City, Philippines, in 2007 and 2009, respectively. He is currently working toward the Ph.D. degree in electrical engineering at the University of New South Wales, Sydney, N.S.W., Australia.

He was with the Electrical and Electronics Engineering Institute, University of the Philippines, Diliman in 2009, where he is currently an Assistant Professor and the Head of the Emerson Network Power Electronics Laboratory from 2012–2013. His current research interests include high-frequency magnetics and power electronics.

Daming Zhang (M'03) received the bachelor's and master's degrees from the Huazhong University of Science and Technology, Wuhan, China, in 1993 and 1996, respectively.

From 1996 to 1997, he was with Guoce Corporation, Wuhan, China. From 1999 to 2003, he was with the Institute of High Performance Computing, Hefei, China. From May 2003 to January 2012, he was with Nanyang Technological University, Singapore, as an Assistant Professor. He is currently a Lecturer at the School of Electrical Engineering and Telecommunication, University of New South Wales, Sydney, N.S.W., Australia. His research interests include characterization of magnetic materials, application of Jiles–Atherton model to study harmonics, conducted EMI, inrush current, transient and nonlinear phenomena in power electronics converters and design of kilohertz to megahertz transformers and inductors for switch-mode power converters. He also has interest in operation and protection of microgrid.

John E. Fletcher (M'11–SM'13) received the B.Eng. (with first-class Hons.) and Ph.D. degrees in electrical and electronic engineering from Heriot-Watt University, Edinburgh, U.K., in 1991 and 1995, respectively.

Until 2007, he was a Lecturer with the Heriot-Watt University. From 2007–2010, he was a Senior Lecturer with the University of Strathclyde, Glasgow, U.K. He is currently a Professor with the University of New South Wales, Sydney, N.S.W., Australia. His research interests include distributed and renewable integration, silicon carbide electronics, pulsed-power applications of power electronics, and the design and control of electrical machines.

Prof. Fletcher is a Charted Engineer in the U.K. and a Fellow of the Institution of Engineering and Technology.